Comparison of $^{13}C_\alpha H$ and ^{15}NH backbone dynamics in protein GB1

DJAUDAT IDIYATULLIN, IRINA NESMELOVA, VLADIMIR A. DARAGAN, AND KEVIN H. MAYO

Department of Biochemistry, Molecular Biology & Biophysics, University of Minnesota, Minneapolis, Minnesota 55455, USA

(RECEIVED August 14, 2002; FINAL REVISION February 3, 2003; ACCEPTED February 12, 2003)

Abstract

This study presents a site-resolved experimental view of backbone $C_\alpha H$ and NH internal motions in the 56-residue immunoglobulin-binding domain of streptococcal protein G, GB1. Using $^{13}C_\alpha H$ and ^{15}NH NMR relaxation data [T_1, T_2, and NOE] acquired at three resonance frequencies (^1H frequencies of 500, 600, and 800 MHz), spectral density functions were calculated as $F(\omega) = 2\omega J(\omega)$ to provide a model-independent way to visualize and analyze internal motional correlation time distributions for backbone groups in GB1. Line broadening in $F(\omega)$ curves indicates the presence of nanosecond time scale internal motions (0.8 to 5 nsec) for all $C_\alpha H$ and NH groups. Deconvolution of $F(\omega)$ curves effectively separates overall tumbling and internal motional correlation time distributions to yield more accurate order parameters than determined by using standard model free approaches. Compared to NH groups, $C_\alpha H$ internal motions are more broadly distributed on the nanosecond time scale, and larger $C_\alpha H$ order parameters are related to correlated bond rotations for $C_\alpha H$ fluctuations. Motional parameters for NH groups are more structurally correlated, with NH order parameters, for example, being larger for residues in more structured regions of β-sheet and helix and generally smaller for residues in the loop and turns. This is most likely related to the observation that NH order parameters are correlated to hydrogen bonding. This study contributes to the general understanding of protein dynamics and exemplifies an alternative and easier way to analyze NMR relaxation data.

Keywords: NMR; relaxation; spectral density; correlation times

The 56 residue immunoglobulin-binding domain of streptococcal protein G (GB1) is an ideal model system with which to investigate protein dynamics by using NMR relaxation. It is a small, yet highly stable (Alexander et al. 1992) (T_m of 87 °C at pH 5.4), well-structured protein (Gronenborn et al. 1991) that is folded as a four-stranded β-sheet (residues 2–8, 13–20, 42–46, and 51–56), on top of which lies an α-helix running from residues 22 to 37 (Fig. 1). GB1 already has been extensively studied in terms of its thermodynamic stability. Over the predenaturation temperature range between 5 and 30°C, the calorimetrically determined free energy of unfolding for GB1 (Alexander et al. 1992) varies little and, on raising the temperature further, falls gradually to zero by 87°C. In this regard, GB1 behaves thermodynamically like a larger protein and, therefore, may be considered representative of any number of proteins.

NMR relaxation provides the only way to derive site-specific dynamics information through the protein sequence. Using multifield measurements of relaxation parameters T_1, T_2, and NOEs, one can obtain many motional parameters related to various bond rotations. Although ^{15}N NMR relaxation has become a standard tool for studying protein dynamics, the picture remains incomplete without knowledge of the internal motions of various CH bonds. Backbone $C_\alpha H$ bond motions reflect correlations of ϕ and ψ dihedral angles and the influence of side-chain χ_1 rotations (Daragan and Mayo 1996a,b; Daragan et al. 1997; Ramirez

Reprint requests to: Kevin H. Mayo, Department of Biochemistry, Molecular Biology & Biophysics, 6-155 Jackson Hall, University of Minnesota, 321 Church Street, Minneapolis, MN 55455, USA; e-mail: mayox001@tc.umn.edu; fax: 612-624-5121.

Article and publication are at http://www.proteinscience.org/cgi/doi/10.1110/ps.0228703.

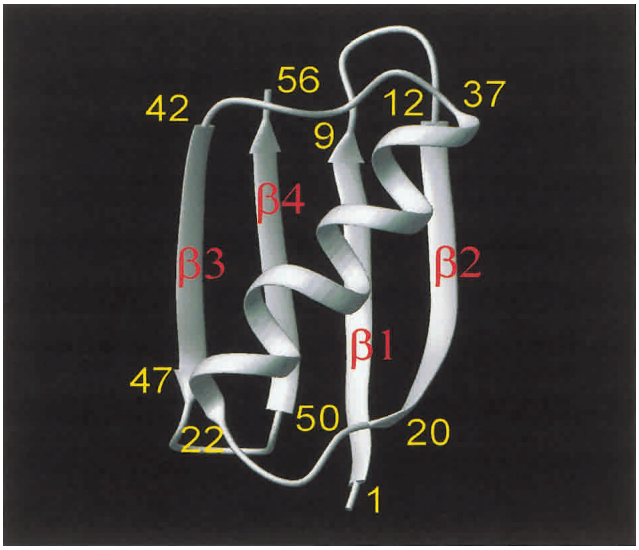

Figure 1. Overall fold for GB1. The overall fold of GB1 is illustrated as given by Gronenborn et al. (1991).

et al. 1998; Idiyatullin et al. 2000). As with NH groups, information on CH internal motions can be derived from analysis of NMR relaxation data. Despite the importance of ^{13}C NMR relaxation studies of proteins, there are few research groups where such measurements are being performed (Daragan et al. 1997; Kemple et al. 1997; A.L. Lee et al. 1997; L.K. Lee et al. 1997; Carr et al. 1998; Hall and Tang 1998; Lee et al. 1998; Yang et al. 1998; Guenneugues et al. 1999; Huang et al. 1999; Walsh et al. 2001). One of the reasons for this is the influence of ^{13}C-^{13}C interactions in uniformly ^{13}C-enriched proteins, which increases line broadening and introduces undesirable contributions to relaxation parameters from ^{13}C -^{13}C dipolar interactions. Nevertheless, these problems can be reduced significantly by using random fractionally ^{13}C-enriched protein.

Once NMR relaxation parameters have been acquired, most researchers analyze their data using the Lipari-Szabo (1982a,b) "model free" approach. The major limitation with using this method for analysis is that it is only valid for isotropic overall tumbling with internal rotational jumps between *n* equivalent states. In actual proteins, a multitude of internal motional correlation times are required to fully describe various bond rotational fluctuations and correlated motions. A novel method was recently developed to avoid many of the problems associated with the standard model free approaches (Idiyatullin et al. 2001). This new approach yields a motional correlation time distribution without assuming the nature of the molecular motions or the number of motional modes, that is, Lorentzians, involved in the dynamics processes. Here, we have used ^{13}C and ^{15}N NMR relaxation data and this new model free approach to examine $^{13}C_\alpha$H and ^{15}NH internal motional modes in protein GB1.

Results

$^{13}C_\alpha$H and ^{15}NH relaxation data were acquired at three frequencies (^{1}H frequencies of 500, 600, and 800 MHz). These results are exemplified in Figure 2 with ^{13}C and ^{15}N NMR relaxation data (T_1, T_2, and {^{1}H}-^{13}C NOE) at 500 and 800 MHz. Using these relaxation data, $F(\omega)$ curves were calculated and motional correlation time distributions are plotted in Figure 3 for residues M1, T11, A26, A34, D40, and A48 in protein GB1. Similarly appearing curves were obtained for all $^{13}C_\alpha$H and ^{15}NH groups of residues throughout the protein. Two observations common to these distributions can be made: (1) $F(\omega)$ curves for $^{13}C_\alpha$H are generally shifted to lower frequency compared to those for ^{15}NH. This is primarily due to increased viscosity of the ^{13}C-enriched protein in D_2O, which results in somewhat slower overall tumbling motions. (2) The maximum of $F(\omega)$, $F(\omega)_{max}$, for $^{13}C_\alpha$H is usually greater than for ^{15}NH.

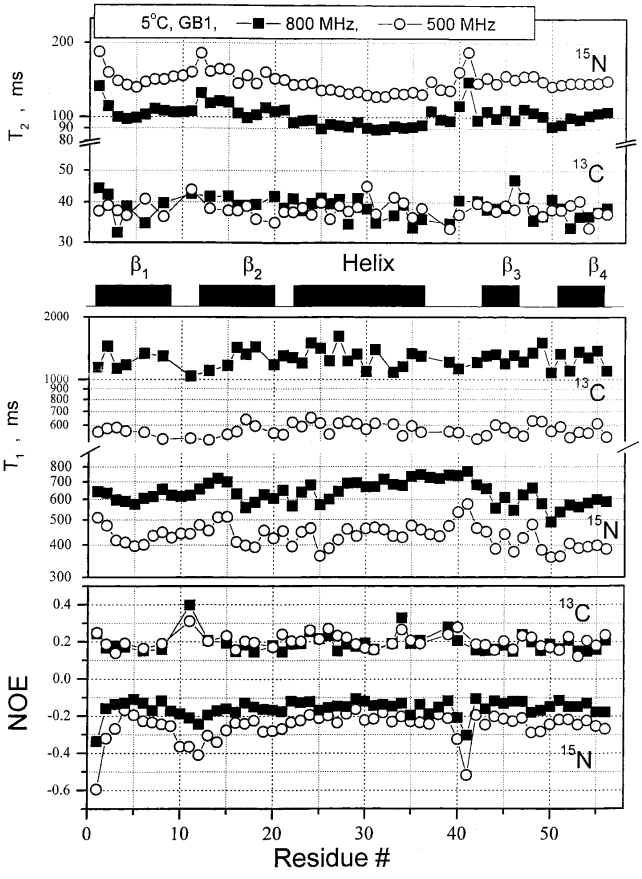

Figure 2. R_1, R_2, and NOE data for protein GB1. ^{13}C and ^{15}N NMR relaxation data [T_1, T_2, {^{1}H}- ^{15}N NOE, and {^{1}H}-^{13}C NOE] on random fractionally ^{13}C-enriched protein GB1 and from a separate sample, uniformly ^{15}N-enriched protein GB1 are plotted versus the GB1 residue number for data acquired at ^{1}H spectrometer frequencies of 500 MHz (open circles) and 800 MHz (filled squares). Secondary structure elements for the protein are given between panels. The temperature for all measurements was 5°C.

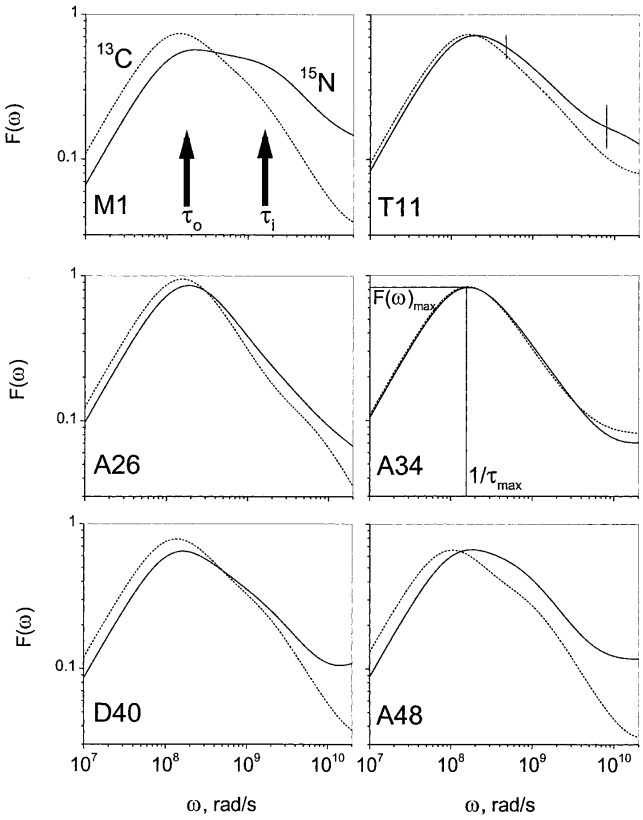

Figure 3. Plots of $F(\omega)$ for six residues in GB1. Because ω is inversely related to the correlation time, $F(\omega)$ gives the distribution of motional correlation times for CH and NH fluctuations over the nanosecond to picosecond range. $F(\omega)$ motional correlation time distributions are exemplified with six CH and NH groups: M1 (β-strand 1), T11 (turn 1), A26 (α-helix), A34 (α-helix), D40 (loop), and A48 (turn 2) through the structure of GB1. Solid lines give $F(\omega)$ curves for ^{15}NH, whereas dotted lines give $F(\omega)$ curves for $^{13}C_\alpha$H. $F(\omega)$ curves were truncated at 100 psec because internal motions occurring on the picosecond time scale are not accurately defined.

As will be discussed below, this results partly from a shift of the $^{13}C_\alpha$H internal motional correlation time distribution closer to that of overall tumbling and partly from correlated bond rotations that influence $^{13}C_\alpha$H fluctuations more than they do those of ^{15}NH.

$F(\omega)_{max}$, labeled in the panel for residue A34, is the maximum height of the $F(\omega)$ curve, and $1/\tau_{max}$ is the corresponding value for the inverse correlation time read from the ω frequency axis. For well-separated overall tumbling and internal motional correlation times, $F(\omega)_{max}$ and τ_{max} would be equivalent to the well-known Lipari-Szabo order parameter, S^2, and overall tumbling correlation time, τ_o, respectively. By visualizing spectral density functions using the $F(\omega)$ approach, it is obvious that this is not the case. This is most evident in the $F(\omega)$ curve for the NH of M1 (Fig. 3), which clearly shows overlapping peaks from at least two motional correlation time distributions on the nanosecond time scale, one for overall tumbling and the other(s) for internal motions. The centers of these distributions are roughly indicated by vertical arrows marked τ_o and τ_i, respectively. In most other $F(\omega)$ curves, shoulders are evident at higher frequency. In these cases, $S^2 < F(\omega)_{max}$ and $\tau_o > \tau_{max}$.

Contributions from multiple Lorentzians was assessed and semiquantified by taking the line width of $F(\omega)$ curves at half-height, 1/2 $F(\omega)_{max}$, a value that has been termed ω_{LR} (Idiyatullin et al. 2001). A single Lorentzian resulting from overall tumbling of a spherical molecule has an ω_{LR} value of 13.93. GB1, however, is ellipsoid in shape with a $D_{||}/D_z$ ratio of 1.8. Because of this, ω_{LR} depends on the orientation of a particular C_α-H and N—H vector within the molecular frame of GB1. Using the program TENSOR II (Daragan and Mayo 1997) and the coordinates for GB1 averaged over 60 NMR-derived structures from the PDB database [accession code: GB1], values of ω_{LR} for C_α-H and N—H vectors in GB1 have been calculated and found to fall generally in the range from about 14 to 15 (Fig. 4A, B). Some vectors are oriented more parallel to the long axis of the molecule, yielding smaller values of ω_{LR}, whereas

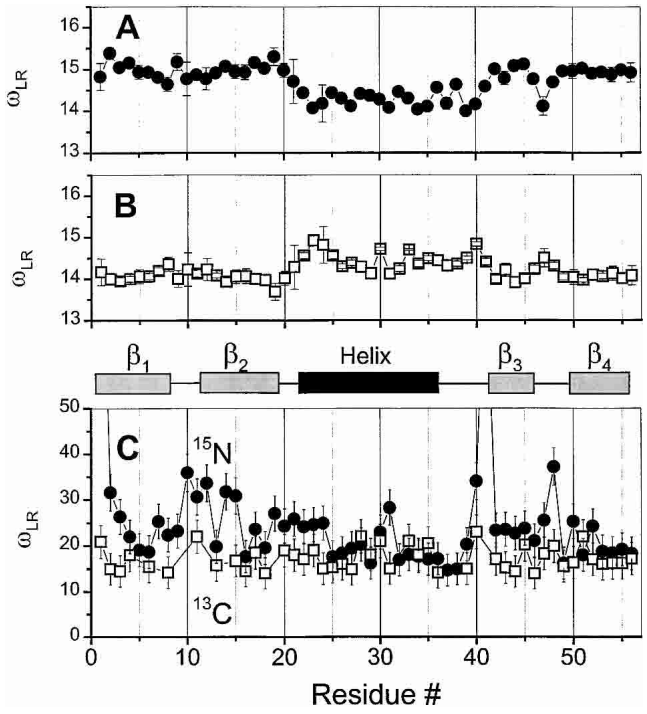

Figure 4. ω_{RL} plotted versus residue number from GB1. Calculated values for ω_{RL} are plotted for CH (*A*) and NH (*B*) vectors in GB1 and for experimentally determined values of ω_{RL} for $^{13}C_\alpha$H (open squares) and for ^{15}NH (filled circles) (*C*). Values of ω_{RL} for C—H and N—H vectors in GB1 were calculated using the program TENSOR II (Daragan and Mayo 1997) and the coordinates for GB1 averaged over 60 NMR-derived structures from the PDB (accession code GB1). Experimentally determined values for ω_{RL} are plotted for 5°C. For calculated values of ω_{RL}, the scale is more expanded to illustrate the effect through the sequence. Secondary structure elements in GB1 are shown between panels.

others are oriented more perpendicular to this axis, resulting in larger values of ω_{LR}. Experimentally determined values for ω_{LR} are plotted versus residue number in Figure 4C. In most cases, the observed ω_{LR} is larger than expected for overall tumbling alone, indicating that the shape of the molecule plays a minor role in this broadening phenomenon. Moreover, the magnitudes of ω_{LR} demonstrate that there are significant contributions to $F(\omega)$ from internal motions occurring on the nanosecond time scale.

Due to the presence of multiple motional modes, the Lipari-Szabo model (Lipari and Szabo 1982a,b) cannot be used to analyze these data. Moreover, even use of the Clore et al. (1990) model, which is limited to three Lorentzians, is questionable because the number of motional modes composing these distributions is unknown. One of the advantages of using the $F(\omega)$ approach is that, without concern for the number of Lorentzians involved in internal motional processes, $F(\omega)$ curves can be deconvoluted into two main components, $F_o(\omega)$ for overall tumbling and $F_i(\omega)$ for the distribution of correlation times associated with internal motions. The deconvolution procedure is described in the Materials and Methods section. Deconvolution of $F(\omega)$ allows one to derive more accurate values for the order parameter, S^2, and overall tumbling correlation time, τ_o, because $F_o(\omega)$ is essentially devoid of contributions from nanosecond time scale internal motions. τ_o values, derived as $1/\omega$ at $F_o(\omega)_{max}$ (data not shown), are generally larger for $^{13}C_\alpha H$ groups than for ^{15}NH groups. This results from increased viscosity due to D_2O in the ^{13}C-enriched protein sample and H_2O in the ^{15}N-enriched protein sample. The residue-averaged τ_o value for $^{13}C_\alpha H$ is 8.2 ns, whereas the residue-averaged τ_o value for ^{15}NH is 6.4 ns. This difference can be explained by hydrodynamic effects because the ratio of these τ_o values is essentially the same as that for the viscosities for D_2O and H_2O.

S^2_{CH} and S^2_{NH} values, plotted in Figure 5, fall approximately between 0.5 and 0.8. S^2_{NH} values appear to be more structurally correlated, with generally lower values being observed for residues located at the N-terminus, the C-terminal part of the helix, and within turns 1 and 2 and the loop. This may have been anticipated because a computational analysis on peptide dynamics using the "internally restricted correlated rotation" (IRCR) model (Daragan and Mayo 1996b) indicates that S^2_{NH} is more sensitive to structural differences than is S^2_{CH}. Moreover, analysis of these data indicates that S^2_{NH} is correlated to hydrogen bonding. In GB1, NHs of 36 out of 56 residues are involved in hydrogen bonds. An average of these S^2_{NH} values is 0.76 ± 0.04, whereas the average S^2_{NH} for all other nonhydrogen bonded NHs, aside from those of the N- and C-terminal residues, is 0.62 ± 0.05. Even when omitting turn and loop residues from the calculation, this difference remains. Another observation is that S^2_{CH} values, for any given residue, tend to be larger than S^2_{NH} values. As will be discussed later, the reason for this is related to more complicated $C_\alpha H$ bond motions involving correlated ϕ, ψ, χ (side-chain) bond rotations.

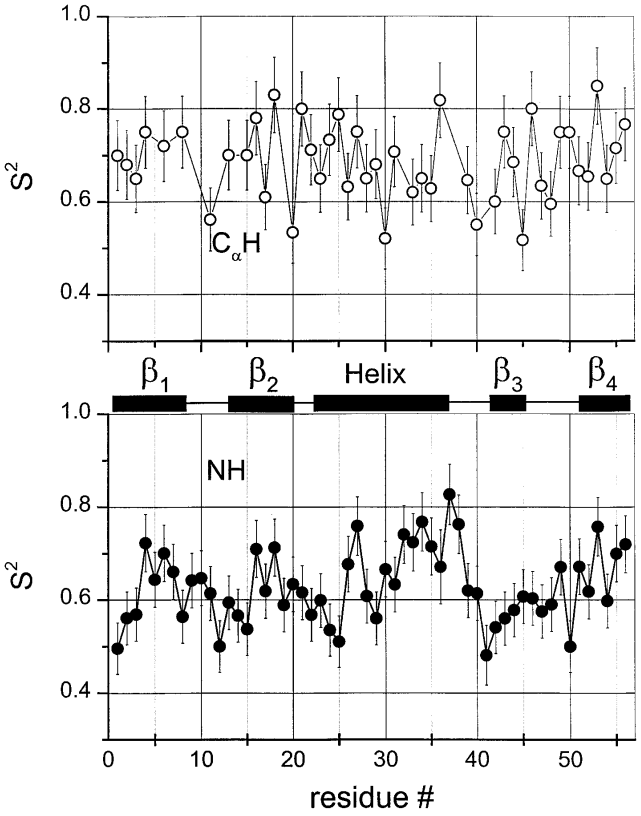

Figure 5. $^{13}C_\alpha H$ and ^{15}NH order parameters versus residue number. Order parameters were obtained using the $F(\omega)$ deconvolution approach as described in the Materials and Methods section. Open circles are for $^{13}C_\alpha H$ and filled circles are for ^{15}NH. Secondary structure elements in GB1 are shown between panels.

Two parameters are key to discussing the $F_i(\omega)$ component: $F_i(\omega)_{max}$, which represents a weighted sum of correlation coefficients for internal motions, and τ_i^R, the value of $1/\omega$ read at $F_i(\omega)_{max}$. Although $F_i(\omega)$ curves represent a rather broad distribution of internal motional correlation times over about two orders in magnitude, analysis and comparison of these nanosecond time scale motions is simplified by using τ_i^R. These internal motional parameters for $^{13}C_\alpha H$ (open circles) and ^{15}NH (filled squares) groups are plotted in Figure 6A and B. $F_i(\omega)_{max}$ values indicate that nanosecond time scale internal motions contribute significantly to the spectral density function, somewhat more so for NH than for $C_\alpha H$. For both $C_\alpha H$ and NH groups, τ_i^R values fall close to each other, lying between 1 and 5 ns. On average, however, τ_i^R is somewhat larger for $C_\alpha H$ than for NH, indicating that $C_\alpha H$ internal motions on the nanosecond time scale are slower and/or are involved in more concerted types of motion.

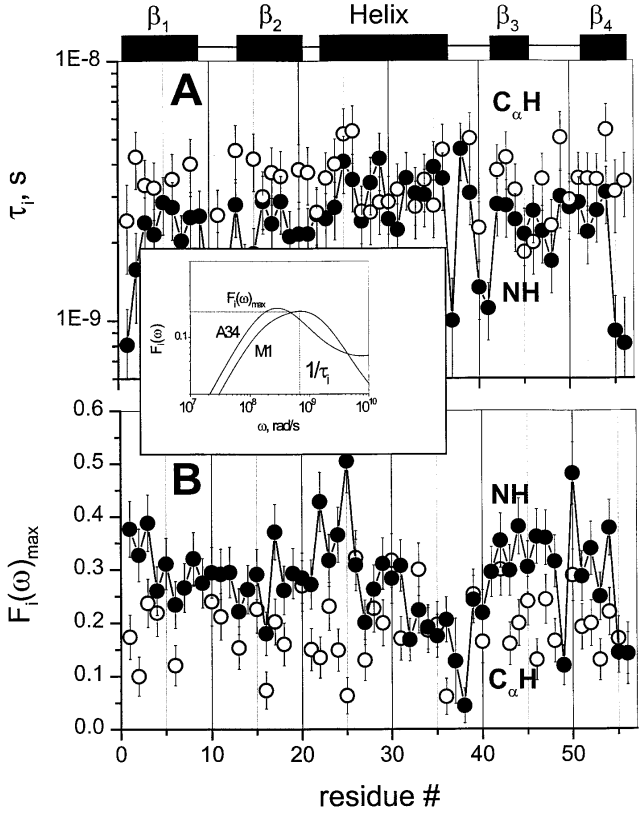

Figure 6. $F_i(\omega)_{max}$ and τ_i^R values plotted versus the residue number. τ_i^R (*A*) and $F_i(\omega)_{max}$ (*B*) values are plotted for $^{13}C_\alpha H$ (open circles) and ^{15}NH (filled squares) versus the GB1 residue number. τ_i^R represents the inverse of the frequency ω at $F_i(\omega)_{max}$. Secondary structure elements in GB1 are shown between panels. The insert exemplifies the function $F_i(\omega)$ for ^{15}NH for two residues M1 and A34 that results from deconvolution of $F(\omega)$ into $F_o(\omega)$ and $F_i(\omega)$.

Discussion

This ^{13}C and ^{15}N NMR relaxation study has presented a comprehensive, site-resolved experimental view of backbone $C_\alpha H$ and NH internal motions in protein GB1. The three primary results of the study are: (1) nanosecond time scale internal motions are observed for all backbone NH and $C_\alpha H$ groups; (2) $C_\alpha H$ internal motions are slower on the nanosecond time scale than are NH internal motions, possibly reflecting the influence of correlated bond rotations; and (3) NH order parameters are correlated to the presence of hydrogen bonding and better reflect structural differences in the protein.

Although a number of ^{15}N NMR relaxation-based studies on protein dynamics have reported the presence of nanosecond time scale internal motions for a few residues (e.g., Clore et al. 1991; Barchi et al. 1994; Mandel et al. 1996; Coles et al. 1999; Berglund et al. 2000; Hidehito et al. 2000; Seewald et al. 2000; Zajicek et al. 2000; Baber et al. 2001; Canet et al. 2001), most protein dynamics studies do not, or perhaps cannot, accurately derive internal motional correlation times, primarily due to the paucity of NMR relaxation data and limitations of the motional model(s) used. In fact, two of these dynamics investigations (Barchi et al. 1994; Seewald et al. 2000) were performed on the same protein GB1, and nanosecond time scale internal motions were reported for only a handful of NHs, and even these were different in each study. Moreover, when internal motions are analyzed, discussion is limited most often to the picosecond time scale. However, even on an 800-MHz NMR spectrometer, the accessible frequency range is limited to about 160 psec and picosecond time scale internal motions (less than about 100 psec) cannot be accurately determined when overall tumbling is much slower than this limiting value, and order parameters are not at their lower limit as for fast internal rotations of methyl groups in side chains (Daragan and Mayo 1996a, 1997, 1998).

Given the present findings with protein GB1, it is plausible that all groups in all proteins undergo nanosecond time scale internal motions. This proposal is consistent with the concept forwarded by Frauenfelder et al. (1991) that there exists a hierarchy of internal motions in proteins. This hierarchy ranges from picoseconds to nanoseconds to microseconds to milliseconds and slower. NMR relaxation studies, which are most sensitive to motions occurring on the nanosecond to picosecond time scales, on small GXG tripeptides devoid of folded structure revealed that internal motions for backbone $C_\alpha H$ and NH groups fall in the 70- to 100-psec range (Mikhailov et al. 1999), whereas in protein GB1, internal motions for backbone groups fall in the subnanosecond to 5-nsec range, as well as in the picosecond range. Internal motions on the picosecond time scale were mostly omitted from this discussion primarily because these faster time scale motions are least accurately determined as mentioned above. Nevertheless, because spectral density functions for GB1 trail into the picosecond range, it is most probable that picosecond time scale internal motions (less than about 100 psec) contribute about 10% or less to the spectral density function. In any event, because of the prevalence of nanosecond time scale internal motions, caution should be exercised by investigators who only use the Lipari-Szabo model free approach to analyze NMR relaxation data. When overall tumbling and internal motions occur on the same time scale, multiple Lorentzians overlap, and this leads to overestimated order parameters and underestimated overall tumbling correlation times when using the Lipari-Szabo approach or any approach that uses fewer Lorentzians than the number of motional modes present. Using the $F(\omega)$ approach avoids this problem.

On the nanosecond time scale, motional fluctuations for $C_\alpha Hs$ are slower than they are for NHs. Slower internal motions for backbone CHs suggest more complicated, concerted types of motions. This interpretation is supported by results on partially folded peptides where NH backbone

motions could be described by motions about a single bond, that is, the C_α-N ϕ-bond, whereas C_αH motions could only be explained fully by considering concerted ϕ, ψ, and χ bond rotations (Ramirez et al. 1998; Idiyatullin et al. 2000). Furthermore, this idea is consistent with the observed larger order parameters for C_αHs compared to those for NHs. The average value for S^2 in β-sheet segments is 0.7 for $^{13}C_\alpha H$ and 0.6 for ^{15}NH, whereas the average value for S^2 for the helix is 0.65 for $^{13}C_\alpha H$ as well as for ^{15}NH. Although most protein dynamics studies interpret S^2 values in terms of restricted motional amplitudes, angular variance is only one contribution to the order parameter. Another is the presence of correlated bond rotations, which can have a significant influence on S^2 (Daragan and Mayo 1996b, 1997). When considering both motional amplitudes and correlated motions, order parameters for C_αH and NH backbone bond motions can be expressed (Daragan and Mayo 1997) as:

$$S^2_{CH} = 1 - R_{CH}{}^2\,(3.9 + 5.3c_{\psi'\phi} - 1.3c_{\phi\psi}) \quad \text{for α-helix structure} \qquad (1a)$$

$$S^2_{CH} = 1 - R_{CH}{}^2\,(5.5 + 5.5c_{\psi'\phi} - 1.3c_{\phi\psi}) \quad \text{for β-strand structure} \qquad (1b)$$

$$S^2_{NH} = 1 - R_{NH}{}^2\,(3.7 - 2c_{\psi'\phi} - 0.1c_{\phi\psi}) \quad \text{for α-helix structure} \qquad (1c)$$

$$S^2_{NH} = 1 - R_{NH}{}^2\,(4.9 + 2c_{\psi'\phi} - 2.7c_{\phi\psi}) \quad \text{for β-strand structure} \qquad (1d)$$

$c_{\phi\psi}$ is the rotational correlation coefficient for ψ_i and ϕ_i backbone rotations; and $c_{\psi'\phi}$ is the rotational correlation coefficient for ψ_{i-1} and ϕ_i backbone rotations, and R^2 is the average squared amplitude of ϕ and ψ rotations [$R^2 = \sigma_\phi\sigma_\psi$]. For a short peptide segment, ψ_i and ϕ_i bonds are illustrated in Figure 7. Notice that order parameters defined in this way (equation 1a–d) are structure dependent. For model peptides conformed in α-helix and β-strand (extended) structures, Daragan and Mayo (1996b) have estimated typical ranges for $c_{\psi'\phi}$ and $c_{\phi\psi}$ correlation coefficients:

α-helix: $c_{\phi\psi}$: range of −0.4 to −0.13 (2a)

$c_{\psi'\phi}$: range of −0.8 to −0.35 (2b)

β-strand: $c_{\phi\psi}$: range of +0.4 to +0.11 (2c)

$c_{\psi'\phi}$: range of −0.95 to −0.6 (2d)

Molecular dynamics calculations on protein GB1 (E. Ermakova, I. Nesmelova, V.A. Daragan, D. Idiyatullin, and K.H. Mayo, unpubl.) show that for most residues, $c_{\phi\psi}$ is closer to zero, whereas $c_{\psi'\phi}$ is largely negative. In any event, the question here is how do these correlation coefficients affect the order parameter. For ^{15}NH motions, correlated backbone motions will always act to minimize S^2_{NH} because $c_{\psi'\phi}$ is always negative. On the other hand, for $^{13}C_\alpha H$ motions, $c_{\phi\psi}$ is negative and $c_{\psi'\phi}$ acts to increase S^2. Because it is reasonable to assume that R^2_{CH} has about the same value as R^2_{NH} (Daragan and Mayo 1997), the observation that S^2_{CH} is greater than S^2_{NH}, especially for β-sheet residues, supports the proposition that C_αH fluctuations are related to correlated bond rotations.

Materials and methods

Protein production

The 56-residue protein GB1 was produced as a recombinant protein as described by Barchi et al. (1994). *Escherichia coli* containing the expression system for GB1 were grown on M9 minimal media containing glucose as the carbon source, 20% of which was uniformly ^{13}C-enriched glucose. The ^{13}C-enriched protein was purified by HPLC using a linear acetonitrile/water gradient, and purity was checked by MALDI-TOF mass spectrometry and analytical HPLC on a C18 Bondclone (Phenomenex) column. For NMR measurements, freeze-dried samples were dissolved in D_2O in 20 mM potassium phosphate. Protein concentration, determined from the dry weight of freeze-dried samples, was 10 mg/mL. The pH was adjusted to pH 5.25 by adding microliter quantities of NaOD or DCl.

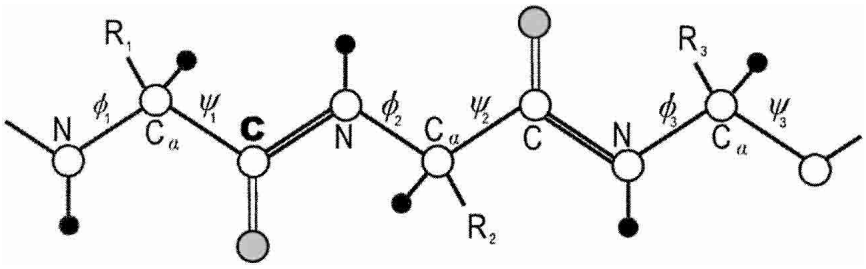

Figure 7. Sketch of peptide backbone. A tripeptide backbone is illustrated to show ϕ and ψ backbone dihedral angles as discussed in the text.

NMR relaxation experiments

With ^{13}C- and ^{15}N-enriched GB1, spin-lattice (T_1), rotating frame spin-lattice ($T_{1\rho}$) relaxation times and heteronuclear NOEs were measured at three Larmor precession frequencies (^1H frequencies of 500, 600, and 800 MHz) on Varian Inova 500, 600, and 800 NMR spectrometers equipped with triple-resonance probes. The temperature was held at 5°C, with calibration being performed by using the chemical shifts of resonances from methanol.

^{13}C and ^{15}N T_1 and $T_{1\rho}$ relaxation times were measured by using the HSQCSE pulse sequence (Yamazaki et al. 1994; Farrow et al. 1995), which employs pulsed field gradients for the coherence transfer pathway whereby magnetization passes from ^1H to ^{13}C (or ^{15}N) and back again to ^1H for observation. To attenuate crosscorrelation between dipolar and chemical-shift anisotropy mechanisms during the relaxation period, an even number of 180° ^1H pulses with alternating phase were applied every 5 msec (Kay et al. 1992; Palmer III et al. 1992). Spectra were recorded by using seven different relaxation delays with values from 10 msec up to $2T_i$, where T_i is the respective relaxation time. For all T_1 and $T_{1\rho}$ experiments, the recycle period was 1.7 sec, and all relaxation curves followed single exponential decay. To prevent ^{13}C-^{13}C scalar and dipolar coupling effects on relaxation parameters (Yamazaki et al. 1994), GB1 was randomly ^{13}C-enriched to only 20%. In this case, residual effects on T_1 values from neighboring ^{13}C groups was less than 5% and negligible for ^{13}C-{^1H}NOEs. This was estimated by comparing relaxation parameters measured using 100% ^{13}C-enriched GB1 and 20% ^{13}C-enriched GB1. For $T_{1\rho}$ relaxation experiments, the carrier for ^{13}C was set at 59 ppm and the frequency of the field lock was 2.6 kHz.

Steady-state {^1H}-^{13}C and {^1H}-^{15}N NOEs were determined from two spectra recorded with proton broadband irradiation and in the absence of proton saturation (Yamazaki et al. 1994; Farrow et al. 1995). Saturation was achieved by application of 120° ^1H pulses applied every 5 msec (Markley et al. 1971) during repetition times of 3 sec.

All experiments were repeated two times for T_1 and $T_{1\rho}$ and four times for NOEs. Average values are reported.

Relaxation data analysis

Because relaxation measurements were performed at high frequency where the influence of chemical shift anisotropy and chemical exchange terms are significant, the square dependence of these terms on the value of the magnetic field was used during the minimization procedure described below. The CSA constants used were −25 ppm for ^{13}C (Peng and Wagner 1994) and −170 ppm for ^{15}N (Tjandra et al. 1996). Moreover, the length of the amide HN bond used in ^{15}N relaxation studies is the subject of an ongoing debate (Korzhnev et al. 2001). Because this work does not propose to solve the problem of NH bond vibrational corrections, a traditional value of 1.02 Å for the length of the N—H bond was used (Kay et al. 1989), which is widely employed by other authors in field.

We have recently developed an approach to analyzing NMR relaxation data, which yields a correlation time distribution for molecular motion without assuming the nature of the molecular motions or the number of motional modes, that is, Lorentzians (Idiyatullin et al. 2001). We introduced the function $F(\omega)$, which is related to the spectral density function as:

$$F(\omega) = 2\omega J(\omega) \tag{3}$$

Although the function $\omega J(\omega)$ is almost equivalent to the imaginary part of the dielectric spectrum as described by Debye (1929) and has been used for many years in various branches of science, we are not aware that it has ever been used to interpret NMR relaxation data as is being done here.

$F(\omega)$ can be represented as the sum of the peaks corresponding to the motional modes, and the spectral density function $J(\omega)$ can be expressed as a sum of Lorentzians:

$$J(\omega) = \frac{c_0\tau_0}{1+\omega^2\tau_0^2} + \frac{c_1\tau_1}{1+\omega^2\tau_1^2} + \ldots \tag{4}$$

If motional correlation times are well separated, positions of peak maxima on the frequency axis, ω, are equal to the inverse of the correlation times $1/\tau_i$ and the peak maxima are equal to the weighting coefficients c_i in equation 4. Although values for c_i and τ_i for $i > 2$ cannot be determined accurately, $F(\omega)$ can be fairly accurately described for any number of Lorentzians. This is due to the fact that during minimization $F(\omega)$ remains stable, even though mutual switching of c_i and τ_i values prevents determination of their specific values. For $J(0) = c_0\tau_0 + c_1\tau_1$, for example, various combinations of c_0, τ_0, c_1, and τ_1 give the same value of $J(0)$. In this regard, $J(0)$ can be determined more accurately than can the individual terms in $J(0)$. The same can be stated for $F(\omega)$, that is, many combinations of c_i and τ_i give the same value of $F(\omega)$ over a wide range of frequencies. These properties of $F(\omega)$ allow the function to be used easily in the interpretation of NMR relaxation data where there are a large number of motional modes.

The largest peak in a $F(\omega)$ curve corresponds to low-frequency motions associated with overall tumbling, and any other peaks or shoulders on the higher frequency side result from the presence of a distribution of internal motional correlation times on the nanosecond and picosecond time scales. The highest frequency peak, that is, picosecond time scale, cannot be determined accurately because the accessible spectrometer frequency range is limited, with a 900-MHz spectrometer, for example, to correlation times in the frequency range up to $2\pi(900 + 225)$ MHz = 7 GHz ($\omega_H + \omega_C$), corresponding to a correlation time of 140 psec. The height of the major peak, $F(\omega)_{max}$, is equal to c_0 in equation 4 when there is no nanosecond time scale internal motions. For molecules tumbling isotropically, the coefficient c_0 can be interpreted as the squared order parameter. However, when nanosecond time scale internal motions are present, Lorentzians for overall tumbling and internal motions overlap and lead to the inequality:

$$F(\omega)_{max} > c_0 = S^2 \tag{5}$$

When τ_o and τ_i are not well-separated, the presence of nanosecond time scale internal motions may be reflected in the half-height line width, ω_{LR}, of the major peak of $F(\omega)$. In effect, $\omega_{LR} = \omega_R/\omega_L$, where ω_R and ω_L are the high- and low-frequency positions taken at the half-height of $F(\omega)$, that is, $F(\omega_R) = F(\omega_L) = 0.5F(\omega)_{max}$. If the spectral density function can be described by a single Lorentzian, then $\omega_{LR} = 13.93$.

Using ^{13}C and ^{15}N relaxation data, $F(\omega)$ curves, which are independent of any motional model, were determined over the frequency range $0 < \omega < 6.28 \times 10^9$ rad/sec by using the Monte Carlo minimization protocol described previously by Idiyatullin et al. (2001) using the program FRELAN (www.nmr-relaxation.com) developed in our lab. Because ω is inversely related to the correlation time, these plots, in fact, give the distribution of motional correlation times over the nanosecond to picosecond range. These distributions are truncated at about 100 psec because of inaccuracies in determining $F(\omega)$ at shorter correlation times, tbat is, higher

frequencies, where actual experimental data are lacking. Three main parameters define $F(\omega)$: $F(\omega)_{max}$, τ_{max}, and ω_{LR}, where τ_{max} is the inverse of the frequency ω at $F(\omega)_{max}$. With well-separated correlation time distributions for overall tumbling and internal motion, τ_{max} will be close to the value of the correlation time for overall tumbling, τ_0. However, if internal motions have correlation times close to τ_0, the value τ_{max} will be less than the value of τ_0.

To obtain parameters related to overall tumbling and internal motion, $F(\omega)$ was deconvoluted into two parts:

$$F(\omega) = c_0 F_0(\omega) + F_i(\omega) \tag{6}$$

where the weighting coefficient, c_0, can be interpreted as the squared order parameter, S^2, and $F_0(\omega)$ contains overall tumbling correlation times:

$$F_0(\omega) = \sum_{k=1}^{N} \frac{2\omega a_k \tau_k}{1 + \omega^2 \tau_k^2} \text{ with } \sum_{k=1}^{N} a_k = 1 \tag{7}$$

and $F_i(\omega)$ contains correlation times for internal motions:

$$F_i(\omega) = \sum_{k=1}^{N} \frac{2c_k \omega \tau_k^R}{1 + (\omega \tau_k^R)^2} \tag{8}$$

To simplify the deconvolution procedure, it was assumed that $F_0(\omega)$ can be described by a single Lorentzian because correlation times in equation 7 are narrowly distributed. In this case, one needs to determine $x = \tau_o$ ($x > \tau_{max}$) to minimize $F_i(\omega)$ for all $\omega < \omega_{max}$ under the condition:

$$1/\tau_k^R = 1/\tau_k - 1/x \tag{9}$$

By doing this, correlation times which are close to τ_o become accentuated and maxima associated with overall tumbling and internal motions become better separated. By deriving $F_i(\omega)$ in this way, the internal motional correlation time distribution can be visualized and the associated parameters $F_i(\omega)_{max}$ and τ_i can be used as general terms to describe internal motions for N—H and C—H vectors.

To calculate $F(\omega)$, one needs to determine the coefficients c_i and correlation times τ_i for $i = 0, 1, \ldots, N$, with N being as large as possible for any given set of experimental data. For example, with three relaxation parameters (e.g., T_1, T_2, and NOE) acquired at three magnetic field strengths, nine fitting parameters, that is, five Lorentzians, can be determined by taking into account that $\Sigma c_i = 1$. Although it is practically impossible to obtain reliable values for c_i and τ_i for $N > 2$, linear combinations and other functions of c_i and τ_i over a given frequency range are very stable and can be determined accurately (LeMaster 1999; Idiyatullin et al. 2001). This is basically the key to obtaining the function $F(\omega)$ from experiment.

One way to calculate $F(\omega)$ is to use the Monte Carlo procedure and a simple step-by-step algorithm outlined below:

1. Randomly take five values of the internal motional correlation time τ_i and amplitudes c_i. To cover a range of possible errors and to account for the influence of rotational anisotropy, t_2 should be about 50 to 70% larger than the estimated overall correlation time τ_o for a given protein molecule. To estimate τ_o, the empirical equation can be used (Daragan and Mayo 1997):

$$\tau_o = (9.18 \times 10^{-3}/T)\exp(2416/T)\, n_R^{0.93} \tag{10}$$

where n_R is the number of residues, and T is the temperature in Kelvin.

2. Using minimization program, find appropriate values c_i and τ_i that best fit the experimental data, that is, minimize the sum of the nine terms:

$$\chi^2 = \frac{1}{9}\Sigma\, (R_j - R_j^{calc})^2/\sigma_i^2 \tag{11}$$

R_j are experimental parameters; R_j^{calc} are calculated parameters, and σ_j are the experimental errors in determining R_j. If $\chi^2 < 1$, then store the set of c_i and τ_i. If $\chi^2 > 1$, then repeat steps 1 and 2. By repeating this process n times, one obtains n sets of c_i and τ_i.

3. For each k-th set of c_i and τ_i, calculate $F(\omega)_k$. The probability P_k of finding the k-th set of c_i and τ_i is (Andrec et al. 1999):

$$P_k = \prod_{j=1}^{9} \frac{1}{\sqrt{2\pi\sigma_j^2}} \exp\left[-\frac{(R_j - R_{jk}^{calc})^2}{2\sigma_j^2} \right] \tag{12}$$

R_{jk}^{calc} are calculated parameters for the k-th set.

4. $5n$-weighted Lorentzians can now be used to describe $F(\omega)$. The average value of $F(\omega)$ and the standard deviation $\Delta(\omega)$ of $F(\omega)$ can be calculated as:

$$F(\omega) = \Sigma\, p_k F(\omega)_k \tag{13a}$$

$$\Delta^2(\omega) = \Sigma\, p_k\, [F(\omega) - F(\omega)_k]^2 \tag{13b}$$

with $p_k = P_k/\Sigma\, P_k$.

Acknowledgments

This work was supported by a research grant from the National Institutes of Health (NIH, GM-58005) and benefited from use of the high field NMR facility at the University of Minnesota. NMR instrumentation was provided with funds from the NSF (BIR-961477), the University of Minnesota Medical School, and the Minnesota Medical Foundation. We also thank Judy Haseman for preparing ^{13}C-and ^{15}N-enriched samples of protein GB1.

The publication costs of this article were defrayed in part by payment of page charges. This article must therefore be hereby marked "advertisement" in accordance with 18 USC section 1734 solely to indicate this fact.

References

Alexander, P., Fahnestock, S., Lee, T., Orban, J., and Bryan, P. 1992. Thermodynamic analysis of the folding of the Streptococcal protein G IgG-binding domains B1 and B2: Why small proteins tend to have high denaturation temperatures. *Biochemistry* **31:** 3597–3603.

Andrec, M., Montelione, G.T., and Levy, R.M. 1999. Estimation of dynamics parameters from NMR relaxation data using the Lipari-Szabo model free approach and Bayesian statistical methods. *J. Magn. Reson.* **139:** 408–421.

Baber, J.L., Szabo, A., and Tjandra, N. 2001. Analysis of slow interdomain motion of macromolecules using NMR relaxation data. *J. Am. Chem. Soc.* **123:** 3953–3959.

Barchi, J.J., Grasberger, B., Gronenborn, A.M., and Clore, G.M. 1994. Investigation of the backbone dynamics of the IgG-binding domain of streptococcal protein G by heteronuclear two-dimensional ^{1}H-^{15}N NMR spectroscopy. *Protein Sci.* **3:** 15–21.

Berglund, H., Olerenshaw, D., Sankar, A., Federwisch, M., McDonald, N.Q., and Driscoll, P.C. 2000. The three-dimensional solution structure and dynamic properties of the human FADD death domain. *J. Mol. Biol.* **302:** 171–188.

Canet, D., Barthe, P., Mutzenhardt, P., and Roumestand, C. 2001. A comprehensive analysis of multifield ^{15}N relaxation parameters in proteins: determination of ^{15}N chemical shift anisotropies. *J. Am. Chem. Soc.* **123:** 4567–4576.

Carr, P.A., Fearing, D.A., and Palmer III, A.G. 1998. 3D accordion spectroscopy for measuring ^{15}N and ^{13}CO relaxation rates in poorly resolved NMR spectra. *J. Magn. Reson.* **32:** 25–33.

Clore, G.M., Szabo, A., Bax, A., Kay, L.E., Driscoll, P.C., and Gronenborn, A.M. 1990. Deviations from the simple two-parameter model free approach to the interpretation of ^{15}N NMR relaxation of proteins. *J. Am. Chem. Soc.* **112:** 4989–4991.

Clore, G.M., Driscoll, P.C., Wingfield, P.T., and Gronenborn, A.M. 1991. Analysis of the backbone dynamics of interleukin-1β using two-dimensional inverse detected heteronuclear ^{15}N-^{1}H NMR spectroscopy. *Biochemistry* **29:** 7387–7401.

Coles, M., Diercks, T., Muehlenweg, B., Bartsch, S., Zoelzer, V., Tschesche, H., and Kessler, H. 1999. The solution structure and dynamics of human neutrophil gelatinase-associated lipocalin. *J. Mol. Biol.* **289:** 139–157.

Daragan, V.A. and Mayo, K.H. 1996a. A novel model-free analysis of ^{13}C NMR relaxation of alanine methyl side-chain motions in peptides, *J. Mag. Reson.* **110:** 164–175.

———. 1996b. Analysis of internally restricted correlated rotations in peptides and proteins using ^{13}C and ^{15}N NMR relaxation data. *J. Phys. Chem.* **100:** 8378–8388.

———. 1997. Motional model analyses of protein and peptide dynamics using ^{13}C and ^{15}N NMR relaxation. *Prog. NMR Spectrosc.* **32:** 63–105.

———. 1998. A simple approach to analyzing protein side-chain dynamics from ^{13}C-NMR relaxation data. *J. Magn. Reson.* **130:** 329–334.

Daragan, V.A., Ilyina, E., Fields, C.G., Fields, G.B., and Mayo, KH. 1997. Backbone and side-chain dynamics of residues in a partially folded β-sheet peptide from PF4. *Protein Sci.* **6:** 355–363.

Debye, P. 1929. *Polar molecules*. Chemical Catalogue Co., New York.

Farrow, N.A., Zhang, O., Szabo, A., Torchia, D.A., and Kay, L.E. 1995. Spectral density function mapping using ^{15}N relaxation data exclusively. *J. Biomol. NMR* **6:** 153–162.

Frauenfelder, H., Sligar, S.G., and Wolynes PG. 1991. The energy landscape and motions of proteins. *Science* **254:** 1598–1603.

Gronenborn, A.M., Filpula, D.R., Essig, N.Z., Achari, A., Whitlow,.M., Wingfield, P.T., and Clore, G.M. 1991. A novel, highly stable fold of the immunoglobulin binding domain of streptococcal protein G. *Science* **253:** 657–660.

Guenneugues, M., Gilquin, B., Wolff, N., Menez, A., and Zinn-Justin, S. 1999. Internal motion time scales of a small, highly stable and disulfide-rich protein: A ^{15}N, ^{13}C NMR and molecular dynamics study. *J. Biomol. NMR* **14:** 47–66.

Hall, K.B. and Tang, C. 1998. ^{13}C relaxation and dynamics of the purine bases in the iron responsive element RNA hairpin. *Biochemistry* **37:** 9323–9332.

Hidehito, T., Hung, F., Li, M., Bredt, D.S., and Zhang, M. 2000. Solution structure and backbone dynamics of the second PDZ domain of postsynaptic density-95. *J. Mol. Biol.* **295:** 225–237.

Huang, K., Ghose, R., Flanagan, J.M., and Prestegard, J.H. 1999. Backbone dynamics of the N-terminal domain in *E. coli* DnaJ determined by ^{15}N- and ^{13}CO-relaxation measurements. *Biochemistry* **38:** 10567–10577.

Idiyatullin, D., Krushelnitsky, A., Nesmelova, I., Blanco, F., Daragan, V.A., Serrano, L., and Mayo, K.H. 2000. Internal motional amplitudes and correlated bond rotations in an α-helical peptide derived from ^{13}C and ^{15}N NMR relaxation. *Protein Sci.* **9:** 2118–2127.

Idiyatullin, D., Daragan, V.A., and Mayo, K.H. 2001. A new approach to visualizing spectral density functions and deriving motional correlation time distributions: Applications to an α-helix-forming peptide and to well-folded protein. *J. Magn. Reson.* **152:** 132–148.

Kay, L.E., Torchia, D.A., and Bax, A. 1989. Backbone dynamics of proteins as studied by ^{15}N inverse detected heteronuclear NMR spectroscopy: Application to staphylococcal nuclease. *Biochemistry* **28:** 8972– 8979.

Kay, L.E., Nicholson, L.K., Delaglio, F., Bax, A., and Torchia, D.A. 1992. Pulse sequences for removal of the effect of cross correlation between dipolar and chemical-shift anisotropy relaxation mechanisms on the measurement of heteronuclear T_1 and T_2 values in proteins. *J. Magn. Reson.* **97:** 359–375.

Kemple, M.D., Buckley, P., Yuan, P., and Prendergast, F.G. 1997. Main chain and side chain dynamics of peptides in liquid solution from ^{13}C NMR: Melittin as a model peptide. *Biochemistry* **36:** 1678–1688.

Korzhnev, D.M., Billeter, M., Arseniev, A.S., and Orekhov, V.Y. 2001. NMR studies of Brownian tumbling and internal motions in proteins. *Prog. Nucleic Magn. Reson. Spectrosc.* **38:** 197–266.

Lee, A.L., Urbauer, J.L., and Wand, A.J. 1997. Improved labeling strategy for ^{13}C relaxation measurements of methyl groups in proteins. *J. Biomol. NMR* **9:** 437–440.

Lee, C.S., Kumar, T.K., Lian, L.Y., Cheng, J.W., and Yu, C. 1998. Main-chain dynamics of cardiotoxin II from Taiwan cobra (Naja naja atra) as studied by carbon-13 NMR at natural abundance: Delineation of the role of functionally important residues. *Biochemistry* **37:** 155–164.

Lee, L.K., Rance, M., Chazin, W.J., and Palmer III, A.G. 1997. Rotational diffusion anisotropy of proteins from simultaneous analysis of ^{15}N and ^{13}C α nuclear spin relaxation. *J. Biomol. NMR* **9:** 287–298.

LeMaster, D.M. 1999. NMR relaxation order parameter analysis of the dynamics of protein side chains. *J. Am. Chem. Soc.* **121:** 1726–1742.

Lipari, G. and Szabo, A. 1982a. Model-free approach to the interpretation of nuclear magnetic resonance relaxation in macromolecules. I. Theory and range of validity. *J. Am. Chem. Soc.* **104:** 4546–4559.

———. 1982b. Model-free approach to the interpretation of nuclear magnetic resonance relaxation in macromolecules. II. Analysis of experimental results. *J. Am. Chem. Soc.* **104:** 4559–4570.

Mandel, A.M., Akke, M., and Palmer, A.G. 1996. Dynamics of ribonuclease H: Temperature dependence of motions on multiple timescales. *Biochemistry* **35:** 16009–16023.

Markley, J.L., Horsley, W.J., and Klein, M.P. 1971. Spin-lattice relaxation measurement in slowly relaxing complex spectra. *J. Chem. Phys.* **53:** 3604–3605.

Mikhailov, D.V., Washington, L., Voloshin, A.M., Daragan, V.A., and Mayo, K.H. 1999. Angular variances for internal bond rotations of side-chains in GXG-based tripeptides derived from ^{13}C-NMR relaxation measurements. *Biopolymers* **49:** 373–383.

Palmer III, A.G., Skelton, N.J., Chazin, W.J., Wright, P.E., and Rance, M. 1992. Suppression of the effect of cross-correlation between dipolar and anisotropic chemical-shift relaxation mechanisms in the measurement of spin-spin relaxation rates. *Mol. Phys.* **75:** 699–711.

Peng, J.W. and Wagner, G. 1994. Investigation of protein motions via relaxation measurements. *Methods Enzymol.* **239:** 563–596.

Ramirez-Alvarado, M., Daragan, V.A., Serrano, L., and Mayo, K.H. 1998. Motional dynamics of residues in a β-hairpin peptide measured by ^{13}C-NMR relaxation. *Protein Sci.* **7:** 720–729.

Seewald, M.J., Pichumani, K., Stowell, C., Tibbals, B.V., Regan, L., and Stone, M.J. 2000. Role of backbone conformational heat capacity in protein stability: Temperature dependent dynamics of the B1 domain of *Streptococcal* protein G. *Protein Sci.* **9:** 1177–1193.

Tjandra, N., Szabo, A., and Bax, A. 1996. Protein backbone dynamics and ^{15}N chemical shift anisotropy from quantitative measurement of relaxation interference effect. *J. Am. Chem. Soc.* **118:** 6986–6991.

Walsh, S.T., Lee, A.L., DeGrado, W.F., and Wand, A.J. 2001. Dynamics of a de novo designed three-helix bundle protein studied by ^{15}N, ^{13}C, and ^{2}H NMR relaxation methods. *Biochemistry* **40:** 9560–9569.

Yamazaki, T., Muhandiram, R., and Kay, L.E. 1994. NMR Experiments for the measurement of carbon relaxation properties in highly enriched, uniformly ^{13}C, ^{15}N-labeled proteins: Application to $^{13}C_{\alpha}$ carbons. *J. Am. Chem. Soc.* **116:** 8260–8278.

Yang, D., Mittermaier, A., Mok, Y.K., and Kay, L.E. 1998. A study of protein side-chain dynamics from new ^{2}H auto-correlation and ^{13}C cross-correlation NMR experiments: Application to the N-terminal SH3 domain from drk. *J. Mol. Biol.* **276:** 939–954.

Zajicek, J., Chang, Y., and Castellino, F.J. 2000. The effects of ligand binding on the backbone dynamics of the kringle 1 domain of human plasminogen. *J. Mol. Biol.* **301:** 333–347.